Research in Astronomy and Astrophysics, 24:015021 (8pp), 2024 January https://doi.org/10.1088/1674-4527/ad05e9

The RFI Fast Mitigation Algorithm Based on Block LMS Filter

Han Wu[1,2], Hai-Long Zhang[1,2,3,4,5], Ya-Zhou Zhang[1,2], Jie Wang[1,4], Xu Du[1,2], Ting Zhang[1,2], and Xin-Chen Ye[1,2,4]
[1] Xinjiang Astronomical Observatory, Chinese Academy of Sciences, Urumqi 830011, China; zhanghailong@xao.ac.cn
[2] University of Chinese Academy of Sciences, Beijing 100049, China
[3] Key Laboratory of Radio Astronomy, Chinese Academy of Sciences, Nanjing 210008, China
[4] National Astronomical Data Center, Beijing 100101, China
Received 2023 September 12; revised 2023 October 16; accepted 2023 October 20; published 2024 January 9

Abstract

The radio telescope possesses high sensitivity and strong signal collection capabilities. While receiving celestial radiation signals, it also captures Radio Frequency Interferences (RFIs) introduced by human activities. RFI, as signals originating from sources other than the astronomical targets, significantly impacts the quality of astronomical data. This paper presents an RFI fast mitigation algorithm based on block Least Mean Square (LMS) algorithm. It enhances the traditional adaptive LMS filter by grouping L adjacent time-sampled points into one block and applying the same filter coefficients for filtering within each block. This transformation reduces multiplication calculations and enhances algorithm efficiency by leveraging the time-domain convolution theorem. The algorithm is tested using baseband data from the Parkes 64 m radio telescope's pulsar observations and simulated data. The results confirm the algorithm's effectiveness, as the pulsar profile after RFI mitigation closely matches the original pulsar profile.

Key words: methods: data analysis – techniques: interferometric – (stars:) pulsars: individual (J0437-4715)

1. Introduction

With increasing radio activity and heightened radio telescope sensitivity, interference from other radio signal sources becomes more likely. Previous researchers have proposed many effective methods to mitigate Radio Frequency Interferences (RFIs). Zhang et al. (2013) proposed establishing a radio-quiet zone for FAST to mitigate the impact of human-made RFI on radio telescopes. Offringa et al. (2010) and Yang et al. (2020) respectively used the SumThreshold method and deep learning algorithms to label RFI in time-frequency domain images. Wang et al. (2021) established a satellite RFI database for the radio telescope's pointing direction using a reference antenna installed on FAST. With improved telescope sensitivity and the growing number of artificial satellites, passive methods like ground-based radio-quiet zones and marking or avoiding RFI are no longer adequate to meet observation demands. Therefore, more scholars have begun exploring more proactive interference mitigation methods, among which adaptive filters are a mature and reliable approach (Morello et al. 2021).

Adaptive RFI suppressors used in the field of astronomy originate from adaptive noise cancellers. In 1965, Kelly at Bell Laboratories was the first to suggest using adaptive filters for phone echo cancellation. Later in 1967, this work was organized and published by Sondhi (1967). Over the years, scholars have attempted to introduce adaptive filtering algorithms into RFI mitigation in radio telescopes. Kesteven et al. (2005) attempted to use adaptive filters to mitigate RFI in pulsar data. Szadkowski (2020) tested the mitigation effect on communication signals using forward prediction error (FPE) filters and Least Mean Square (LMS) filters on a cosmic-ray detector. Finger et al. (2018) attempted real-time RFI mitigation for the FAST using adaptive filters.

In practical applications, the convergence time of adaptive filters is influenced by factors such as circuit frequency, algorithm complexity, and filter order. In previous work, Szadkowski (2021) achieved a convergence time of approximately 500 μs, while Finger et al. (2018) achieved a convergence time (at $1/e$) of approximately 27 μs. Reducing the number of multiplication calculations can effectively reduce hardware resource consumption and save computational time.

To address issues such as high resource consumption, computational complexity, and asynchronous phases of two interfering signals in the adaptive RFI mitigation process, this paper presents an RFI fast mitigation algorithm based on block adaptive LMS filters.

2. Design of the RFI Fast Mitigation Algorithm

Let the interference signal emitted by the interference source be represented as v'. The unknown channels between the interference source and the radio telescope, as well as the reference antenna, are represented as $w_{\rm ast}$ and $w_{\rm ref}$. If the RFI measured by the reference antenna is v_2, the interference signal measured by the radio telescope is $\frac{w_{\rm ast}}{w_{\rm ref}}v_2$. Using the unknown

[5] Author to whom any correspondence should be addressed.

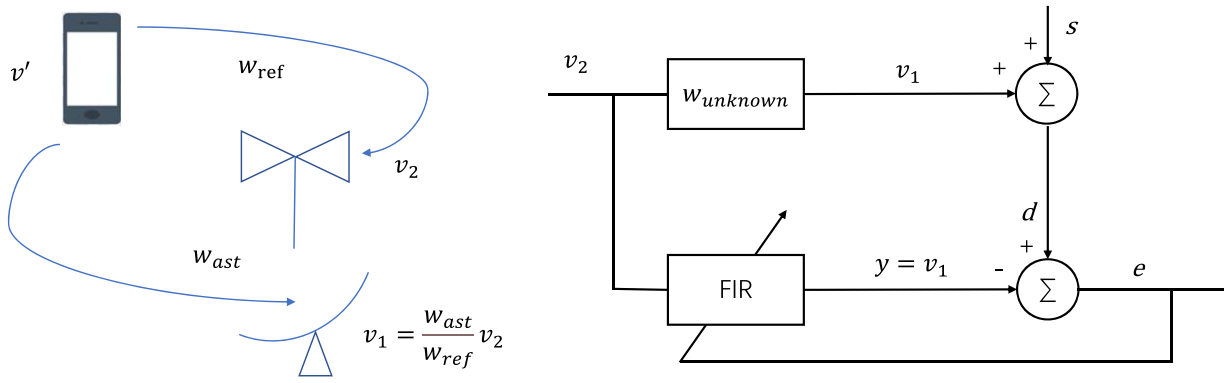

Figure 1. RFI enters the reference antenna and radio telescope through different paths (left), using the RFI received by the reference antenna as a reference. The difference between the RFI measured by the reference antenna and that measured by the radio telescope, denoted as $\frac{w_{\text{ast}}}{w_{\text{ref}}}$, is abstracted as w_{unknown}. This transformation converts the noise cancellation problem into a system identification problem (right).

channel w_{unknown} to represent $\frac{w_{\text{ast}}}{w_{\text{ref}}}$, the noise cancellation problem is transformed into a system identification problem. This transformation indicates that the high correlation between the interference signals in the reference antenna and the radio telescope arises from their common source. The minor distinctions arise because the signals have traversed different channels, and distinct receivers react differently to the same signal. In Figure 1, s represents the astronomical signal, e represents the error signal, and v_1 represents the interference signal measured by the radio telescope. In this problem, it is assumed that the interference signal is uncorrelated with the astronomical signal, and w_o represents the Wiener solution of the system, given as:

$$w_o = \frac{w_{\text{unknown}} \cdot v_2^H \cdot v_2}{v_2^H \cdot v_2} \tag{1}$$

Here the superscript H represents *Hermitian* transpose, Equation (1) and all symbols "·" used in the remainder of this paper represent the multiplication operator. When the adaptive LMS filter operates optimally, the output $y = v_2 \cdot w_o^H = v_2 \cdot w_{\text{unknown}}^H = v_1$ resulting in $e = s$, which means that in ideal conditions, RFI can be completely eliminated to obtain a clean astronomical signal.

$$\begin{aligned} y(n) = &[w_0(n) \;\; w_1(n) \;\; \cdots \;\; w_{M-1}(n)] \\ &\cdot [u(n) \;\; u(n-1) \;\; \cdots \;\; u(n-M+1)]^T \end{aligned} \tag{2}$$

$$d(n) = s(n) + v_1(n) \tag{3}$$

$$e(n) = d(n) - y(n) \tag{4}$$

$$\begin{bmatrix} w_0(n+1) \\ w_1(n+1) \\ \vdots \\ w_{M-1}(n+1) \end{bmatrix} = \begin{bmatrix} w_0(n) \\ w_1(n) \\ \vdots \\ w_{M-1}(n) \end{bmatrix} + \mu \begin{bmatrix} u(n) \\ u(n-1) \\ \vdots \\ u(n-M+1) \end{bmatrix} e^*(n) \tag{5}$$

Let us consider an adaptive LMS filter with an order denoted as M, and the current sample index marked as n. Equation (2) presents the relationship between the output of the LMS filter and its input, where u represents the filter's input data, specifically the interference signal v_2 received by the reference antenna in this context. The superscript T signifies matrix transpose. Equation (3) relates the expected signal d to astronomical signals s and the interference signals v_1 measured by the radio telescope. Equation (4) illustrates the relationship between the error signal e, the expected signal d, and the filter's output y. Equation (5) outlines the coefficient update formula for the LMS filter, with μ representing the step size, typically a small positive value. From Equations (2) to (5), we can compute that processing L data points using an adaptive LMS filter of order M requires $2LM$ multiplications. To reduce algorithmic complexity, this paper introduces the block adaptive LMS algorithm (Walzman & Schwartz 1973) into the RFI mitigation problem.

$$\begin{bmatrix} u(kL) & \cdots & u(kL-M+1) \\ u(kL+1) & & u(kL-M+2) \\ \vdots & \ddots & \vdots \\ u(kL+L-1) & \cdots & u(kL+L-M) \end{bmatrix} \cdot \begin{bmatrix} w_0(k) \\ w_1(k) \\ \vdots \\ w_{M-1}(k) \end{bmatrix} = \begin{bmatrix} y(kL) \\ y(kL+1) \\ \vdots \\ y(kL+L-1) \end{bmatrix} \tag{6}$$

$$\boldsymbol{d}(n) = \boldsymbol{s}(n) + \boldsymbol{v}_1(n) \tag{7}$$

$$\boldsymbol{e}(n) = \boldsymbol{d}(n) - \boldsymbol{y}(n) \tag{8}$$

$$\begin{bmatrix} w_0(k+1) \\ w_1(k+1) \\ \vdots \\ w_{M-1}(k+1) \end{bmatrix} = \begin{bmatrix} w_0(k) \\ w_1(k) \\ \vdots \\ w_{M-1}(k) \end{bmatrix} + \mu \begin{bmatrix} u(kL) & u(kL-1) & \cdots & u(kL-M+1) \\ u(kL+1) & u(kL) & & u(kL-M+2) \\ \vdots & & \ddots & \vdots \\ u(kL+L-1) & u(kL+L-2) & \cdots & u(kL+L-M) \end{bmatrix}^H \cdot \begin{bmatrix} e^*(kL) \\ e^*(kL+1) \\ \vdots \\ e^*(kL+L-1) \end{bmatrix} \tag{9}$$

A segment of data with a length of L is extracted to form a block. Within each block, L input vectors share the same filter coefficients, now represented as $L \times 1$ vectors. k denotes the block number, and the physical meanings of $\boldsymbol{d}$, $\boldsymbol{s}$, $\boldsymbol{v}_1$, $\boldsymbol{e}$ and $\boldsymbol{y}$ remain the same, though they are now in the form of $L \times 1$ vectors. Equation (6) describes the relationship between the filter's output and its input. Equations (7) and (8) express the same meanings as Equations (3) and (4), albeit now in the form of $L \times 1$ vectors. Equation (9) provides the filter's coefficient update Equation.

Equation (6) illustrates the connection between the input and output of a block filter. Each row in the input matrix represents the input vector derived after sampling data at the current time step, and all rows in the input matrix use the same filter coefficient matrix. When the input matrix has only one row, Equation (6) simplifies to the scenario discussed in Equation (2). While Equation (9) involves the linear correlation between the filter input signal and the error signal. According to the time-domain convolution theorem, the FFT (Fast Fourier Transform) can be used to replace matrix multiplication, effectively reducing the number of multiplication operations. This transforms the block-based adaptive LMS filter into a fast block-based adaptive LMS filter.

$$\boldsymbol{W}(k) = \mathrm{FFT}([w_0(k) \;\; w_1(k) \;\; \cdots \;\; \boldsymbol{0}]^T) \tag{10}$$

$$\boldsymbol{U}(k) = \mathrm{FFT}([u(kL-M) \;\; \cdots \;\; u(kL-1) \;\; u(kL) \;\; \cdots \;\; u(kL+L-1)]^T) \tag{11}$$

In Equations (10) and (11), $\boldsymbol{W}$ and $\boldsymbol{U}$ are $(L+M) \times 1$ vectors, $\boldsymbol{0}$ is a $1 \times L$ zero vector, and symbols like k, w, L, T and others represent the same meanings as before. FFT[...] represents fast Fourier transformation applied to the data within the brackets.

$$\boldsymbol{y}(k) = \mathrm{IFFT}(\boldsymbol{U}(k) \odot \boldsymbol{W}(k)) \text{ last } L \text{ elements} \tag{12}$$

In Equation (12), $\odot$ denotes element-wise vector multiplication, also known as the *hadamard* product. IFFT[...] represents inverse fast Fourier transformation applied to the data within the brackets. Utilizing the properties of the overlap-save method and circular convolution, the result of linear convolution is the last L values of the inverse fast Fourier transformation, hence $\boldsymbol{y}$ is an $L \times 1$ vector.

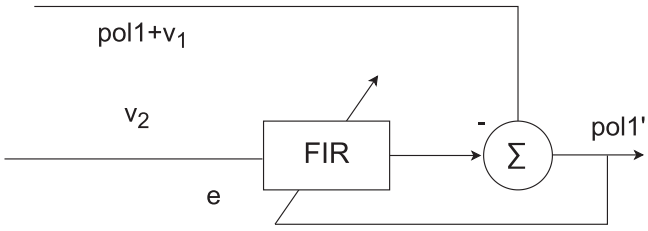

Figure 2. Adaptive RFI suppressor.

Table 1
Basic Information of Experimental Data

Parameter	Value
Source	J0437-4715
Center Freq	1382 MHz
Bandwidths	400 MHz
Nbit	8
Npol	2
Dm	2.64467 cm^{-3} pc
Tsamp	$1/(2*400)$ μs
Instrument	CASPSR

$$\boldsymbol{E}(k) = \mathrm{FFT}([\boldsymbol{0} \;\; e(kL) \;\; \cdots \;\; e(kL+L-1)]^T) \tag{13}$$

$$\phi(k) = \mathrm{IFFT}(\mathrm{conj}(\boldsymbol{U}(k)) \odot \boldsymbol{E}(K)) \text{ first } M \text{ elements} \tag{14}$$

$$\boldsymbol{W}(k+1) = \boldsymbol{W}(k) + \mu \cdot FFT \begin{bmatrix} \phi(k) \\ \boldsymbol{0} \end{bmatrix} \tag{15}$$

In Equation (13), $\boldsymbol{E}$ is an $(L+M) \times 1$ vector, but the difference is that a $1 \times M$ zero vector $\boldsymbol{0}$ is added before $\boldsymbol{e}$. conj() denotes the conjugate of all elements within the brackets. Let ϕ be the cross-correlation matrix between the filter input signal and the error signal. By using properties of inverse discrete Fourier transform and cross-correlation, the result of the cross-correlation operation is the first M values of the inverse fast Fourier transform. Therefore, ϕ is an $M \times 1$ vector. In Equation (10), $\boldsymbol{W}$ is an $(L+M) \times 1$ vector, so in Equation (15), an $L \times 1$ zero vector $\boldsymbol{0}$ is added. The computation from Equation (10) to (15) yields the multiplicative complexity required for M-order filter output data at L points, denoted as $5(L+M) \cdot \log(L+M) + 8(L+M)$(Shynk 1992). In this paper, when both the block length and filter order are set to 512, the fast block-based adaptive LMS filter requires only about $1/9$ of the multiplications compared to the adaptive LMS filter. However, the fast block-based adaptive LMS filter incurs some tracking performance loss since it

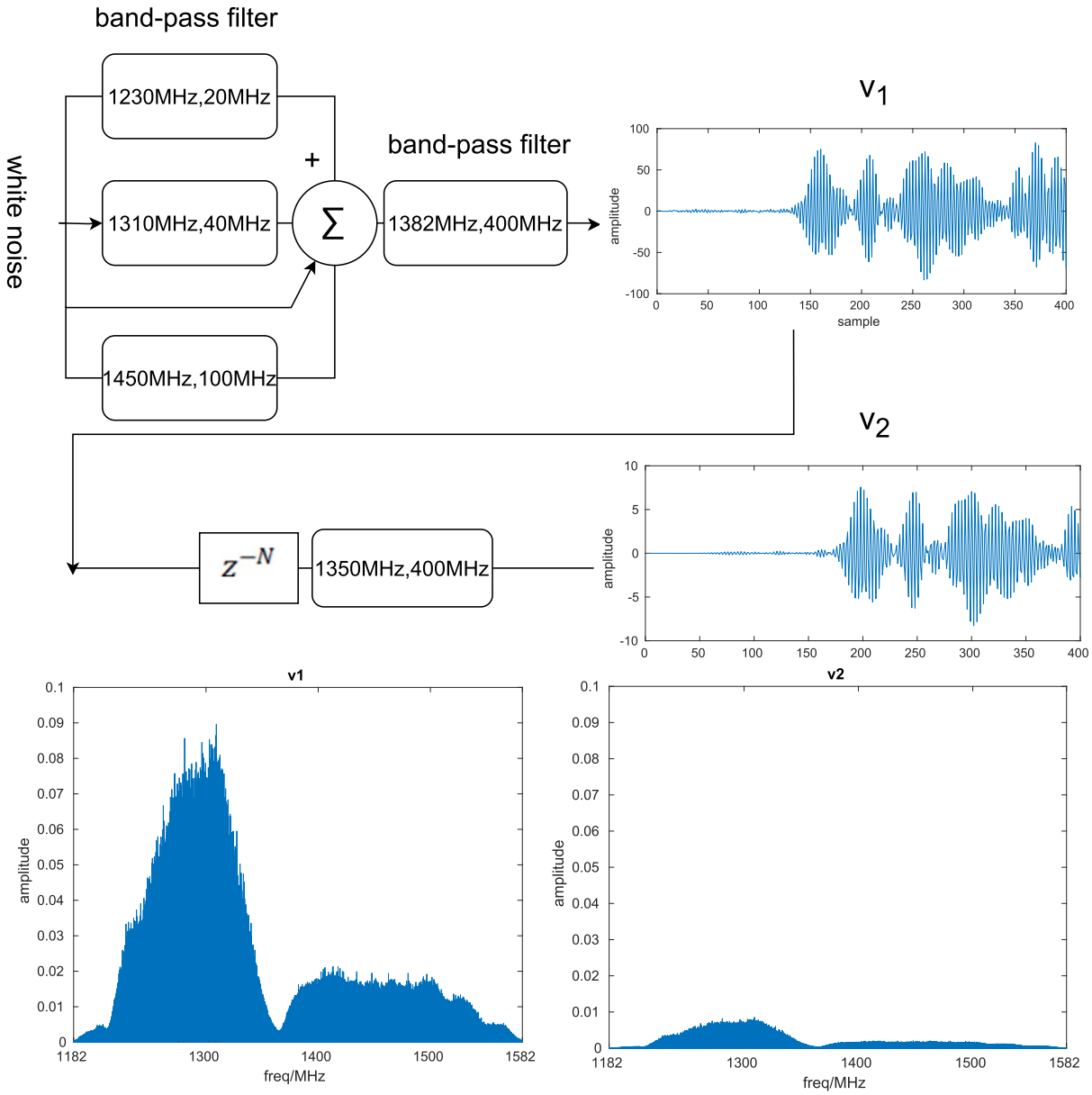

Figure 3. Interference signal generation process (above), spectrum of the interference signal received by the radio telescope (bottom left), and spectrum of the interference signal received by the reference antenna (bottom right).

updates the filter coefficients only once for every L data points, in contrast to the adaptive LMS filter. In practical applications, it is crucial to carefully balance filter tracking performance and algorithm complexity while selecting an appropriate block length. According to the algorithm complexity formula, however, when hardware resources are limited and the filter order is not high, the reduction in algorithm complexity with the use of block-based adaptive LMS filter is quite limited. For instance, if the filter order is only 128 and data of the same length, 512, is being processed, the algorithm complexity is only reduced by approximately 3.75 times.

Previously, the primary method for mitigating RFI was "channel blanking," which removed the entire channel data affected by RFI. This approach traded bandwidth for signal-to-noise ratio, rendering it ineffective when facing broadband interference. Furthermore, adaptive algorithms, while similar to AI algorithms, demand lower computational resources and can handle a greater volume of astronomical data with limited hardware resources.

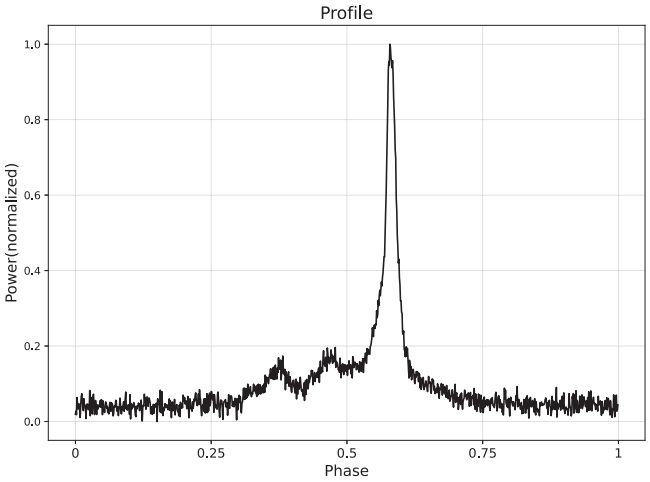

Figure 4. Parkes single-polarization pulsar profile.

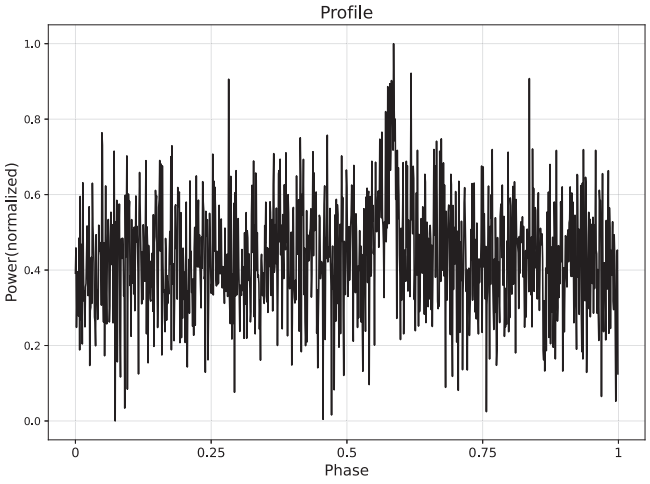

Figure 5. Pulsar profile containing RFI.

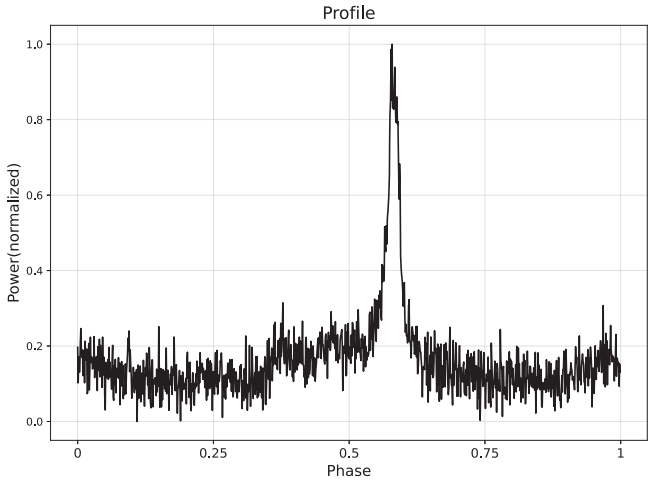

Figure 6. Pulsar profile after RFI mitigation with phase correction.

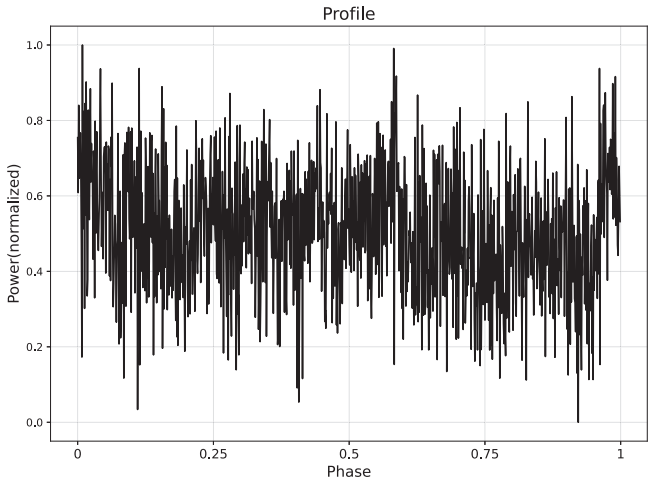

Figure 7. Pulsar profile after RFI mitigation without phase correction.

3. Experimental Environment

The experiment utilized baseband data obtained from the 64 m Parkes radio telescope in Australia during the observation of the pulsar J0437-4715 on 2011 October 29. The basic information of the observed data is presented in Table 1, with an observation duration of approximately 8 s and a data size of 12.8 GB.

In the simulation experiment, $2^{22} \times 1000$ data points from polarization 1 of J0437-4715 were used, corresponding to an observation duration of approximately 5.24288 s. The astronomical signal *pol*1 in Figure 2 corresponds to s in Figure 1, and $pol1'$ represents the output after adaptive RFI mitigation. The radio frequency interference v_1 and v_2 are generated through a software simulation process as shown in Figure 3, while the meanings of the other symbols remain the same as previously mentioned.

In Figure 3, the power of white noise is 100 mW. The rounded rectangular boxes represent bandpass filters, with the first data inside each box indicating the center frequency of the bandpass filter, and the second data indicating the bandwidth of the bandpass filter. There are three bandpass filters with center frequencies of 1230, 1310, and 1450 MHz, designed to generate Gaussian noise with different center frequencies and widths. The gains of these three filters are all positive. Figure 3 employs a bandpass filter with a center frequency of 1382 MHz to simulate the frequency response of a radio telescope to interference signals, resulting in interference signal v_1 received by the radio telescope. v_1 is then delayed by N points and passed through a bandpass filter with a center frequency of 1350 MHz to simulate the interference signal v_2 measured by the reference antenna. In Figure 3, the N-point delay is used to simulate the phase difference between the interference signals

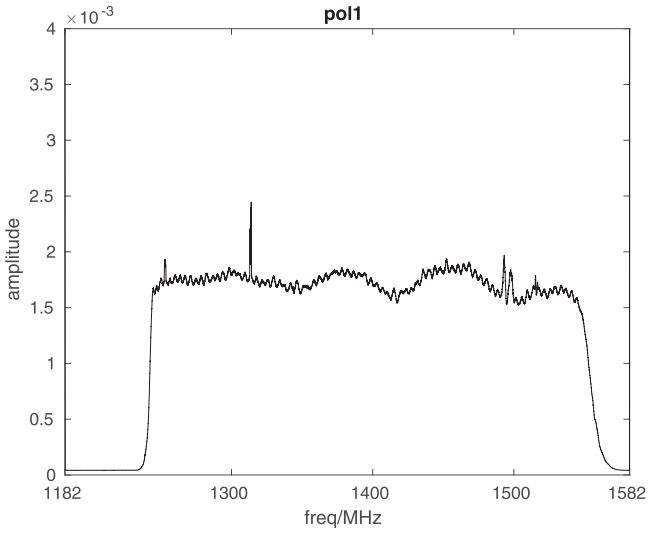

Figure 8. Frequency spectrum of the original pulsar signal.

measured by the radio telescope and the reference antenna. The bandpass filter is used to simulate the frequency response differences between the reference antenna and the radio telescope. Since the aperture of the reference antenna is significantly smaller than that of the radio telescope, the gain of the bandpass filter is negative here.

3.1. Phase Preprocessing

In the context of adaptive RFI mitigation, synchronization between the interference signals measured by the reference antenna and the radio telescope is crucial. Without synchronization, the RFI mitigation problem could become an RFI prediction problem, and prediction problems often yield less satisfactory results compared to mitigation problems.

In practical observations, the distances to the radio telescope and the reference antenna from the interference source may differ, resulting in unsynchronized interference signals. One possible approach is to select the first P sampled points from both the radio telescope and reference antenna for cross-correlation. The x-coordinate of the maximum value in the correlation function represents the number of sampling points for phase offset between signals. Using this fixed phase offset, the leading signals in v_2 and $pol1 + v_1$ can be delayed for alignment.

$$P_{\max\_\text{delay}} = \left\lceil \frac{S_{\text{T\&R}}}{c} \cdot f_s \right\rceil \tag{16}$$

Equation (16) provides the maximum number of points for phase offset when the positions of the radio telescope and reference antenna are fixed. In this case, the number of points P used for cross-correlation must exceed the maximum phase offset points. Here, $P_{\max\_\text{delay}}$ represents the maximum number of points for phase offset between the two interference signals, $S_{\text{T\&R}}$ is the distance between the radio telescope and reference antenna, c is the propagation speed of electromagnetic waves in the medium, f_s is the sampling rate, and $\lceil\rceil$ denotes rounding up to the nearest integer.

3.2. Experimental Steps

1. Divide the CASPSR baseband data into 10 blocks and perform interference mitigation separately for each block. Each block contains $2^{22} \times 100$ data points.
2. Simulate the generation of RFI signals received by the radio telescope and the reference antenna: v_1 and v_2, where each generated interference signal has the same length as the input baseband signal, and the specific generation process is shown in Figure 3.
3. Combine interference signal v_1 with the observation signal $pol1$ to obtain the adaptive filter reference input $pol1 + v_1$, and use v_2 as the filter input signal.
4. Select the first P sampled points for preprocessing, calculate the phase offset point number N, and delay the leading signal by N points.
5. Apply the fast block-based adaptive LMS filter with an order and block length of 512 for adaptive RFI filtering. After each iteration, save the filter output data and coefficient vector. These saved coefficients become the initial values for the next iteration, with the initial coefficients being a zero vector for the first iteration.
6. Read the 10 filter output data files one by one, perform operations such as dispersion removal, folding, and integration to obtain the final pulsar profile.

4. Results Analysis

The pulsar data for J0437-4715 contain two polarization signals. In this experiment, only one polarization data ($pol1$) was used. After undergoing dispersion removal, folding, integration, and other operations, the original pulsar profile was obtained (Zhang et al. 2023), as shown in Figure 4. After adding interference to the original astronomical signal, the resulting signal $pol1 + v_1$ undergoes dispersion, folding, integration, and other operations to generate a pulsar profile image containing RFI, as shown in Figure 5.

To illustrate the impact of phase correction on RFI mitigation, the first block of data ($2^{22} \times 100$ samples) was used for RFI mitigation separately with and without phase correction. After applying dispersion, folding, and integration operations to the two sets of data, we obtained Figures 6 and 7.

Plot the frequency spectrum of the original astronomical signal $pol1$, the astronomical signal with RFI $pol1 + v_1$, and the output signal $pol1'$ after RFI fast mitigation. Comparing the frequency spectrum in Figures 8, 9, and 10, it is observed that

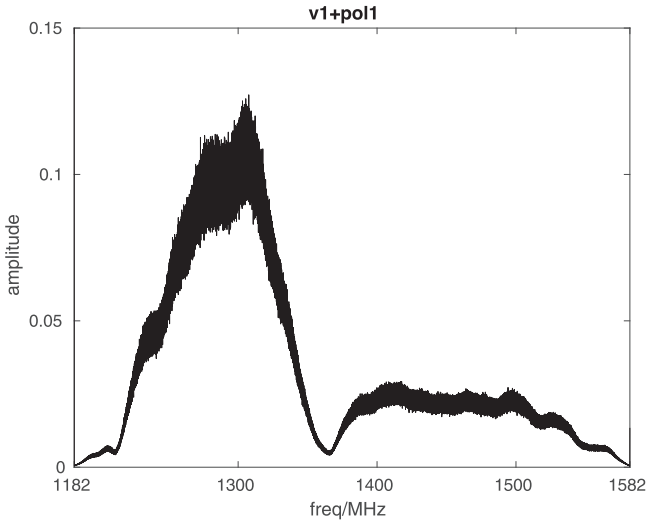

Figure 9. Frequency spectrum of the pulsar signal with RFI.

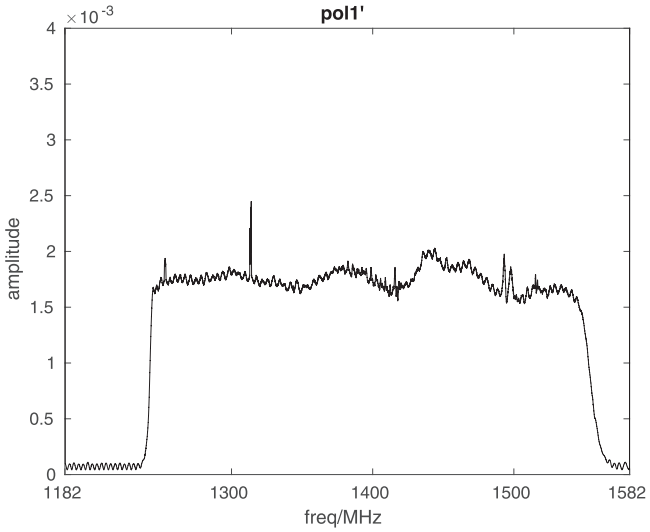

Figure 10. Frequency spectrum of the pulsar signal after interference mitigation.

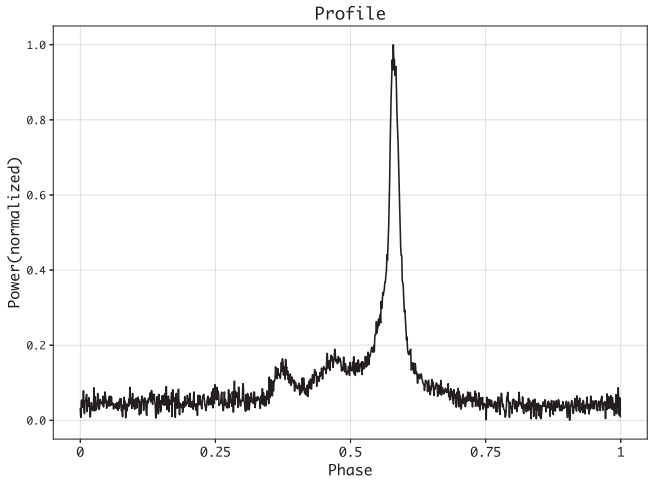

Figure 11. Pulsar profile after RFI fast mitigation.

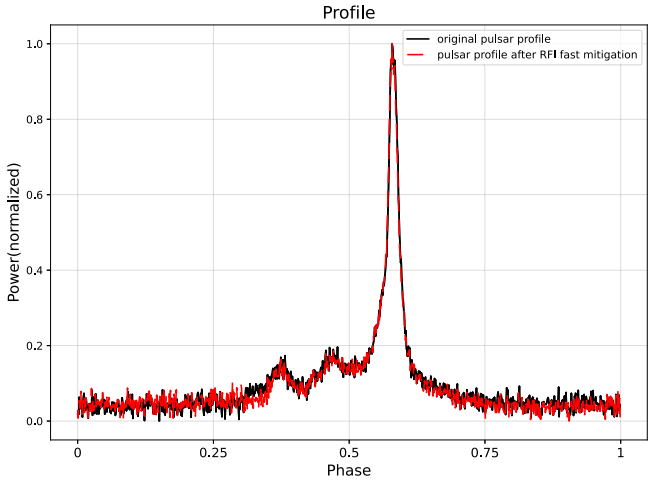

Figure 12. Comparison between the pulsar profile after RFI fast mitigation and the original pulsar profile.

the spectrum after RFI mitigation closely matches the spectrum of the original astronomical signal.

Combine the obtained data from all 10 blocks of *pol*1′, perform dispersion, folding, integration, and other operations to obtain the pulsar profile after RFI mitigation, as shown in Figure 11. A comparison between Figures 11 and 5 reveals the effective mitigation of interference signals by the RFI fast mitigation algorithm. When comparing the pulsar profile after RFI fast mitigation with the original pulsar profile, as depicted in Figure 12, we observe nearly identical phase and amplitude characteristics.

5. Conclusions

This paper addresses the issue of resource consumption and high computational complexity in the adaptive RFI mitigation process by proposing a block-based adaptive RFI fast mitigation algorithm. Simulated experiments were conducted using baseband pulsar data observed with the Australian Parkes 64 m radio telescope, simulated RFI data, and their combination. When comparing the spectra and profiles before and after interference mitigation, it is clear that the block-based adaptive RFI fast mitigation algorithm effectively reduces wideband interference in the baseband data, even when the two interference signals differ. Through theoretical calculations,

compared to the traditional LMS algorithm, the proposed block-based adaptive RFI fast mitigation algorithm reduces the number of multiplications by approximately 9 times when the block length and filter order are set to 512, significantly improving computational efficiency. This paper also introduces a new preprocessing method for the issue of unsynchronized phase between two interference signals and provides a lower bound for the preprocessing data length. Comparing the folded and integrated pulse profiles, the interference mitigation results are improved after phase correction.

Acknowledgments

This work is supported by the National Key R&D Program of China (Nos. 2021YFC2203502 and 2022YFF0711502); the National Natural Science Foundation of China (NSFC) (12173077 and 12073067); the Tianshan Innovation Team Plan of Xinjiang Uygur Autonomous Region (2022D14020); the Tianshan Talent Project of Xinjiang Uygur Autonomous Region (2022TSYCCX0095); the Scientific Instrument Developing Project of the Chinese Academy of Sciences (grant No. PTYQ2022YZZD01); China National Astronomical Data Center (NADC); the Operation, Maintenance and Upgrading Fund for Astronomical Telescopes and Facility Instruments, budgeted from the Ministry of Finance of China (MOF) and administrated by the Chinese Academy of Sciences (CAS); Natural Science Foundation of Xinjiang Uygur Autonomous Region (2022D01A360); the CAS "Light of West China" program under No.2022-XBQNXZ-012. This work is supported by Astronomical Big Data Joint Research Center, co-founded by National Astronomical Observatories, Chinese Academy of Sciences.

ORCID iDs

Hai-Long Zhang https://orcid.org/0000-0002-8951-7094
Ya-Zhou Zhang https://orcid.org/0000-0001-6046-2950
Jie Wang https://orcid.org/0000-0003-0380-6395
Xu Du https://orcid.org/0000-0001-6448-0822

References

Finger, R., Curotto, F., Fuentes, R., et al. 2018, PASP, 130, 1
Kesteven, M., Hobbs, G., Clement, R., et al. 2005, RaSc, 40, RS5S06.1
Morello, V., Rajwade, K. M., & Stappers, B. W. 2021, MNRAS, 510, 1393
Offringa, A. R., de Bruyn, A. G., Biehl, M., et al. 2010, MNRAS, 405, 155
Shynk, J. 1992, ISPM, 9, 14
Sondhi, M. M. 1967, BSTJ, 46, 497
Szadkowski, Z. 2020, ITNS, 67, 405
Szadkowski, Z. 2021, NIMPA, 999, 165171
Walzman, T., & Schwartz, M. 1973, ITIT, 19, 59
Wang, Y., Zhang, H.-Y., Hu, H., et al. 2021, RAA, 21, 18
Yang, Z., Yu, C., Xiao, J., & Zhang, B. 2020, MNRAS, 492, 1421
Zhang, H., Nan, R., Peng, B., et al. 2013, in 2013 Asia-Pacific Symp. on Electromagnetic Compatibility (APEMC) (Melbourne: IEEE), 1
Zhang, H.-L., Zhang, Y.-Z., Zhang, M., et al. 2023, RAA, 23, 015023